Modelling the Earth's gravity field using wavelet frames

I. Panet, O. Jamet, M. Diament, A. Chambodut

▶ **To cite this version:**

I. Panet, O. Jamet, M. Diament, A. Chambodut. Modelling the Earth's gravity field using wavelet frames. Gravity, Geoid and Space Missions, 2004 IAG International Symposium, International Association of Geodesy, Aug 2004, Porto, Portugal. pp.48-53, 10.1007/3-540-26932-0_9 . hal-02612194

HAL Id: hal-02612194
https://hal.science/hal-02612194v1

Submitted on 20 May 2020

HAL is a multi-disciplinary open access archive for the deposit and dissemination of scientific research documents, whether they are published or not. The documents may come from teaching and research institutions in France or abroad, or from public or private research centers.

L'archive ouverte pluridisciplinaire **HAL**, est destinée au dépôt et à la diffusion de documents scientifiques de niveau recherche, publiés ou non, émanant des établissements d'enseignement et de recherche français ou étrangers, des laboratoires publics ou privés.

Modelling the Earth's gravity field using wavelet frames

I . Panet [1,2], O. Jamet [1]
[1] Laboratoire de Recherche en Géodésie, Institut Géographique National, France

M. Diament [2]
[2] Laboratoire de Gravimétrie et Géodynamique, Département de Géophysique Spatiale et Planétaire, Institut de Physique du Globe de Paris, France

A. Chambodut [3]
[3] Laboratoire de Géomagnétisme et Paléomagnétisme, Institut de Physique du Globe de Paris, France

Abstract Present and forthcoming satellite gravity missions provide us with new and unique datasets in order to model the Earth's gravity field at 100 km resolution. These new models will bring significant advances in our understanding of the Earth's structure and dynamics. However, it will be necessary to combine satellite data with surface and airborne measurements in order to improve the short wavelength components of the gravity field. The derived regional models with an increased spatial resolution will be used to carry out geodynamic studies at lithospheric or crustal scale. Whereas the classical spherical harmonics decomposition leads to strong numerical difficulties when dealing with local features, wavelet-based representations can handle the local scales as well as the global ones; they should thus be extremely useful to derive local models taking into account data of different origins. Here we describe the construction of wavelet frames on the sphere based on the Poisson multipole wavelet. Those wavelets are of special interest for field modelling since their shape is linked to the potential of multipole sources, and their scaling parameter to the multipole depth (Holschneider et al., 2003). We also compute a local wavelet decomposition of the gravity field at high resolution from evenly and unevenly distributed data using least squares collocation. Our first results show the efficiency of such a representation.

Keywords Spherical wavelets, multipoles, frame, covariances.

1 Introduction

Gravity field observation from space provides promising advances for improving measurement of the geoid at 100 km resolution, and of its time variations at 400 km resolution. The derived models of the static and time-varying gravity field will lead to a better understanding of the internal geodynamic processes and of the superficial fluid envelops. They will also contribute to improve global and national height references. However, it will be necessary to densify them locally with surface and airborne measurements in order to improve their resolution for local studies. If the spherical harmonic analysis is well suited for global representations, it is very demanding for such high resolution models since the number of functions involved is quite large. Moreover, the systems to solve are badly conditioned when the data do not cover the whole sphere. That is the reason why other methods have been investigated last years: orthonormalization of the spherical harmonics over a bounded domain (Albertella et al., 1999; Hwang, 1993), spherical cap harmonic analysis (de Santis et al.,1997), and a promising approach: wavelet frames (Freeden et al., 1998; Holschneider et al., 2003).

Discrete wavelet frames are based on the discretization of the continuous wavelet transform on the sphere. Many mother wavelets can be used, and among them, axisymmetric wavelets are of special interest. Indeed, they can be expressed in a simple way as series of Legendre polynomials. In the present paper, we focus on a particular family of axisymmetric wavelets, well-suited for modelling of potential fields: the Poisson multipole wavelets. Let us notice that wavelets based on the Poisson kernel were already used in one or two dimensions to analyse and interprete gravity and magnetic anomalies (Sailhac et al., 2000, Martelet et al., 2001).

Contrary to the spherical harmonics basis, wavelet frames are not made of orthonormal functions. Thus, computing the dual frame is required in order to derive the covariances between wavelet coefficients involved in collocation. We finally derive local representations underlining the interest of wavelets for regional, high resolution modelling.

2 Frames of wavelets

2.1 Frames

A collection of functions $\{g_n\}_{n=0,1,...}$ in a Hilbert space H is a frame of H if we have for all $s \in H$:

$$A\|s\|^2 \leq \sum_n |\langle g_n, s\rangle|^2 \leq B\|s\|^2 \quad (1)$$

The constants $(0 < A \leq B < \infty)$ are called frame-bounds, and $\langle g_n, s\rangle$ denotes the scalar product of g_n with s. Such a family provides a complete and stable representation of the space H, which may be redundant. $s \in H$ can be written as:

$$s = \sum_n \langle s, \tilde{g}_n\rangle \; g_n \quad (2)$$

where $\{\tilde{g}_n\}_{n=0,1,...}$ is the dual frame (see section 3.2). When $A = B$, the frame is tight. No direction of space H is privileged. In the opposite case, A and B reflect the extremal sensitivities of the frame.

In the following, the space H is the space of square integrable functions on the unit sphere (admitting an harmonic continuation outside this sphere). The considered frames are spherical wavelet frames. The wavelets are characterized by a scale parameter, defining their spectral content, and a position parameter, defining the point around which they concentrate their energy in space domain. We discretize the continuous wavelet transform via these two parameters. Scales are discretized in order to cover the whole spectrum. For each chosen scale, we discretize the positions in order to cover the whole sphere homogeneously. This defines successive generations j of wavelets.

2.2 The Poisson multipoles wavelets

The Poisson multipole wavelets, introduced by Holschneider et al. (2003), are of special interest for potential field modelling. Indeed, their shape may be identified with the potential of a multipolar source. The wavelet $\psi_i^{a,n,\vec{e}}$ at point $\vec{x}$ on the unit-sphere is expressed as:

$$\psi_i^{a,n,\vec{e}}(\vec{x}) = N_i \sum_\ell (a\ell)^n e^{-a\ell} Q_\ell \left(\frac{\vec{e}}{\|\vec{e}\|} \cdot \vec{x} \right) \quad (3)$$

with :

$$N_i \;\; = \;\; \left(\langle \psi_i^{a,n,\vec{e}}(\vec{x}), \psi_i^{a,n,\vec{e}}(\vec{x}) \rangle \right)^{-\frac{1}{2}} \quad (4)$$

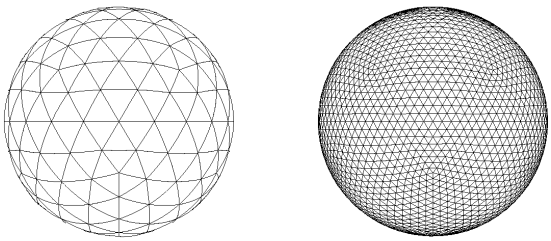

Figure 1: Meshes at generations 3 (*left*) and 5 (*right*).

Its harmonic continuation at point $\vec{x}$ outside the sphere $\Psi_i^{a,n,\vec{e}}$ is given by:

$$\Psi_i^{a,n,\vec{e}}(\vec{x}) = \quad (5)$$
$$N_i \sum_\ell \frac{1}{\|\vec{x}\|^{\ell+1}} (a\ell)^n e^{-a\ell} Q_\ell \left(\frac{\vec{e}}{\|\vec{e}\|} \cdot \frac{\vec{x}}{\|\vec{x}\|} \right)$$

In the above equations, N_i is a L_2-normalisation factor, ℓ is the degree of the Legendre polynomial P_ℓ and Q_ℓ is the related reproducing kernel: $Q_\ell = \frac{2\ell+1}{4\pi} P_\ell$. a is the scale parameter, $\vec{e}$ is the position of the multipole, and n its order. Increasing n improves the frequency localization but deteriorates the space localization. The depth of the multipole in the case of the unit sphere is linked to the scale parameter by $\|\vec{e}\| = e^{-a}$.

2.3 Discretization of scales and positions

We chose a simple sampling of the sphere, based on the successive subdivisions of the facets of a regular convex polyhedron centred with respect to the sphere. The directions of the vertexes are then projected onto the sphere. The more we subdivide the polyhedron's facets, the finer the mesh: thus, we create easily a set of hierarchical meshes associated with wavelets at different scales. The polyhedron chosen is the icosahedron, since it leads to very regular meshes, as shown by Figure 1 (the dispersion of distances between points comes to about 10% of the mean value). The construction of an icosahedric mesh was implemented based on C^{++} code from Richard J. Bono freely distributed on *http://www.applied-synergetics.com*, following Kenner (1976).

To provide a regular coverage of the spectrum, we discretize the scale parameter according to a geometric progression: the scale a_j at level j is given by: $a_j = C.\gamma^{j-1}$. We chose $C = 3$ and $\gamma = \frac{1}{2}$. Thus, the spectrum is covered (see Figure 2); and the multipoles regularly sample the Earth's interior.

The number of wavelets for each scale is large enough so that the wavelet set shows a good sensitivity

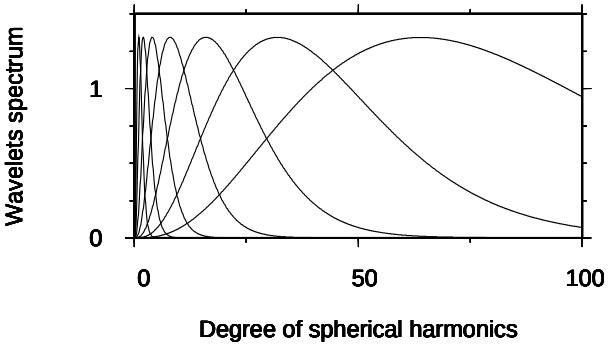

Figure 2: Spectrum of the wavelets $(a_j \ell)^n e^{-a_j \ell}$ as a function of spherical harmonic degree ℓ for generations $j = 1$ to $j = 7$ of the wavelet frame (order $n = 3$ multipoles).

to all degrees and orders of the spherical harmonics. Figure 3, presented in Sect. 3, can be interpreted as a mean number of wavelets per degree/order taking into account a spectral ponderation: the observed values are clearly larger than 1 (case of the spherical harmonics basis) and never tend to 0.

2.4 Frames of spherical wavelets

We did not prove that the above family of wavelets is actually a frame of H. In particular, results describing appropriate discretizations of positions via fundamental systems for band-limited wavelets (Freeden, 1998) can not be applied to wavelets with an infinite spectrum. However, numerical tests seem to support the hypothesis that the wavelet set is a frame (see for instance Sect. 3.2). In any case, the wavelet family provides an approximation of the gravity field. Its quality depends on the generating properties of the wavelets. Thus, a bad representation of the gravity field can be symptomatic of ungenerated harmonic spaces whereas a good one guaranties that the wavelets at least numerically generate those spaces. Numerical tests (Chambodut et al., submitted) at a global scale show that the first generations of wavelets numerically generate spherical harmonics. Given the process of construction of the wavelets set, one can reasonably assume the next generations to show the same approximating properties.

3 Collocation in the non-orthogonal case

Our aim is to derive a high resolution wavelet model of the disturbing potential based on gravity disturbances data. In this section, we derive the collocation formulas in the general frame settings.

3.1 Deriving a model from observations

Taking into account the multipolar nature of the wavelets, we express the disturbing potential T as a linear combination of wavelets:

$$T = \sum_i \alpha_i \Psi_i \tag{6}$$

Thus, wavelet coefficients can be interpreted as a ponderation of multipolar sources. Gravity disturbances δg are hereafter deduced in the spherical approximation:

$$\delta g = \sum_i \alpha_i \frac{\partial \Psi_i}{\partial r} \tag{7}$$

or, in matricial notation: $\delta g = M \cdot \alpha$. α is the vector of unknown coefficients, M the observation matrix. We denote b the vector of measurements (of gravity disturbances). The solution vector is given after Moritz (1989):

$$\alpha = K \cdot M^t (M \cdot K \cdot M^t + W)^{-1} \cdot b \tag{8}$$

where W is the covariance matrix of the noise of the measurements and K the covariance matrix of the coefficients, detailed in the following.

3.2 Dual frame

If the wavelets set is a frame, the coefficients are defined as the scalar products between restriction of the disturbing potential to the unit sphere T_Σ and the dual frame: $\alpha_i = \langle T_\Sigma, \tilde{\psi}_i \rangle$. The dual frame is given by (Mallat, 1999):

$$\tilde{\psi}_i = (U^* U)^{-1} \psi_i \tag{9}$$

where U is the operator defined by:

$$\forall i, \ \ \forall s \in H, \ \ Us[i] = \langle s, \psi_i \rangle \tag{10}$$

and U^* its adjoint. This definition is equivalent to: $\langle \psi_j, \tilde{\psi}_i \rangle = \delta_{ij}$ when the wavelets set is independant.

However, the computation of the dual frame based on the above relationship is computationally demanding, unless the frame is tight. Indeed, a tight frame with frame-bounds equal to A verifies:

$$\tilde{\psi}_i = \frac{1}{A} \psi_i \tag{11}$$

We provide here a qualitative argument supporting the hypothesis that the described wavelet family is close to be tight. We already discussed the generating properties of the wavelet set. In this section, we focus on its isotropy in the space H. Let us define E_m^ℓ as:

$$E_m^\ell = \sum_i |\langle \psi_i, Y_m^\ell \rangle|^2 \tag{12}$$

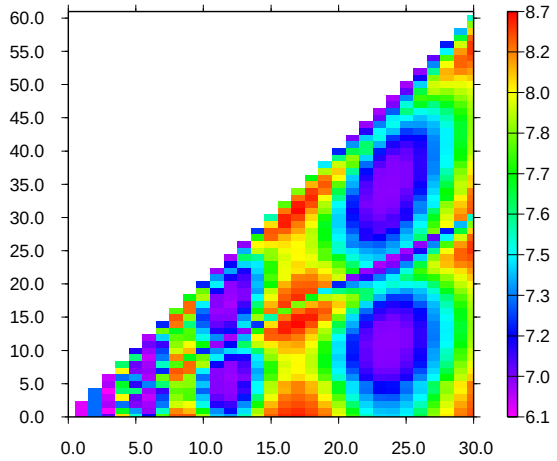

Figure 3: Value of E_m^ℓ for the first 7 generations of wavelets, for all degrees and orders lower than 30. *Abscissa* : degree of spherical harmonics, *ordinate* : order of spherical harmonics.

E_m^ℓ increases when the redundancy of the wavelet family $(\psi_i)_i$ in the direction of the spherical harmonic Y_m^ℓ increases. A necessary condition for the frame to be tight is that E_m^ℓ be constant. This condition is not sufficient. Though, since the directions Y_m^ℓ sample regularly the directions of H, we consider that it supports the tightness hypothesis. Figure 3 plots the values of E_m^ℓ taking into account the first 7 generations of wavelets: they are all coming around 7.5, with relative variations of 18%. Adding further scales would not change this result significantly since the next generations of wavelets have almost no power at degrees lower than 30. Thus, the wavelet set is rather isotropic in the directions Y_m^ℓ, and we assume the framebounds to be close. Further experimental results will confort this hypothesis.

3.3 Covariance matrix K

Thus, we computed the covariances between wavelet coefficients applying the tight frame approximation. We denote $K(\vec{r}, \vec{r_1})$ the covariance function of gravity disturbances at points $\vec{r}$ and $\vec{r_1}$ on the sphere. We make the assumption that $K(\vec{r}, \vec{r_1})$ only depends on the spherical distance between $\vec{r}$ and $\vec{r_1}$. In this case, it can be written as a series of Legendre polynomials after Moritz (1989):

$$K(\vec{r}, \vec{r_1}) \quad = \quad \sum_\ell c_\ell P_\ell(\vec{r} \cdot \vec{r_1}) \qquad (13)$$

The coefficients c_ℓ are equal to the variance of gravity anomalies for degree ℓ. We assume that the power spectrum of the gravity potential follows Kaula's rule of quadratic decrease (Kaula, 1966). Thus, the power spectrum of the gravity disturbance at degree ℓ decreases as:

$$c_\ell \quad = \quad (\ell+1)^2(2\ell+1)\frac{\alpha}{\ell^4} \qquad (14)$$

Let us now denote $K_{\vec{r},\vec{r_1}}$ the operator associating to each square integrable function on the sphere f its scalar product with $K(\vec{r}, \vec{r_1})$:

$$K_{\vec{r},\vec{r_1}} f(\vec{r_1}) \quad = \quad \langle K(\vec{r}, \vec{r_1}), f(\vec{r}) \rangle \qquad (15)$$

We derive the covariance between two coefficients α_i and $\alpha_{i'}$ as a scalar product between the corresponding wavelets. This comes from the formulas of covariance propagation:

$$K_{i,i'} \quad \approx \quad \frac{1}{A^2} \langle K_{\vec{r},\vec{r_1}} \psi_i(\vec{r_1}), \psi_{i'}(\vec{r_1}) \rangle \qquad (16)$$

4 Results

4.1 Data

In this section, we derive wavelet models of the gravity field applying our approach. The studied area is in the northern part of the Andes. Synthetic datasets are obtained by sampling the EGM96 gravity disturbances model from Lemoine et al. (1998). We applied a gaussian filtering to the coefficients up to degree 360 (with an attenuation of 0.6 at degree 250) in order to avoid artificial oscillations. We considered 2 datasets, the one made of regularly distributed data, the other made of randomly distributed data. The regular distribution of data counts 1369 samples, with one data per bin of $0.25°$ in the area of $-5°/-14°$ lat. N, and $278°/287°$ long. E. The irregular one counts 576 samples between $0°/-18°$ lat. N, and $275°/293°$ long. E. The concentration of data is higher in the northern half (394 data) whereas the southern half is more sparsely covered (182 data).

4.2 Parameters

We inverted these datasets on generations 2 to 8 of the frame for the case of irregular data distribution (1920 wavelets), and 2 to 10 for the case of regular data distribution (7189 wavelets). Indeed, since gravity disturbances have no component on degree 1, we do not expect the first generation of wavelets (mainly centred on degree 1) to be significant in the representation. We applied a spatial selection of the wavelets : only wavelets whose influence radius intersects the area under study are selected. The influence radius of a wavelet is based on its spatial variance as defined by Freeden (1998).

Matrix W is diagonal, assuming an uncorrelated noise. As the data are perfect, the choice of W is arbitrary. We considered a noise of 10^{-2} mGals for the regular distribution and $2.5\ 10^{-3}$ mGals for the irregular one. The covariance matrix K is evaluated assuming that $\tilde{\psi}_i = \frac{1}{7.5}\psi_i \ \ \forall i$. Lastly, the filter applied to the synthetic data is taken into account within the observation equations.

4.3 Results

Results for the regular case are presented in Figure 4. Wavelets succeed in representing the local gravity disturbances. Wavelet model shows visually no difference with the EGM 96 model. Residuals between synthetic data and wavelet model amount to a few microGals. Residuals between the EGM 96 model and the wavelet model are of same order that measurements residuals in the central part of the area. We could not avoid small edge effects, around 0.1 to 0.2 mGals, due to the spatial selection of the wavelets. A possible explanation is that the vertices of the meshes show a slight obliquity with respect to meridians and parallels, thus, two edges out of four are privileged. However, this issue still has to be investigated in more details.

Results for the irregular case are presented in Figure 5. The wavelets handle the gaps without oscillating, and restitute the main features of the gravity disturbances. Residuals between synthetic data and wavelet model mainly amount to a few tens of microGals. Residuals between the EGM 96 model and the wavelet model are smaller in the norther part of the area, reflecting the higher density of data. They increase in the areas of strong gravity variations since the available data do not constrain sufficiently the model.

5 Conclusion

These tests proved the ability of a subset of the wavelet frame to represent the gravity field at a rather high resolution in a delimited area, and to cope with an irregular distribution of data. They validate the approximations made in the estimation of the dual frame. The frame used here may be too redundant: good results were also obtained in the regular case with less wavelets (4607 wavelets only). Lastly, let us notice that the wavelet coefficients can be interpreted for geophysical purposes, the generations 1 to 10 corresponding to multipoles located at varying depths from the core up to the Earth's crust. Applying this method, we intent to derive local refinements of the global gravity model from current and planned space missions by jointly modelling two

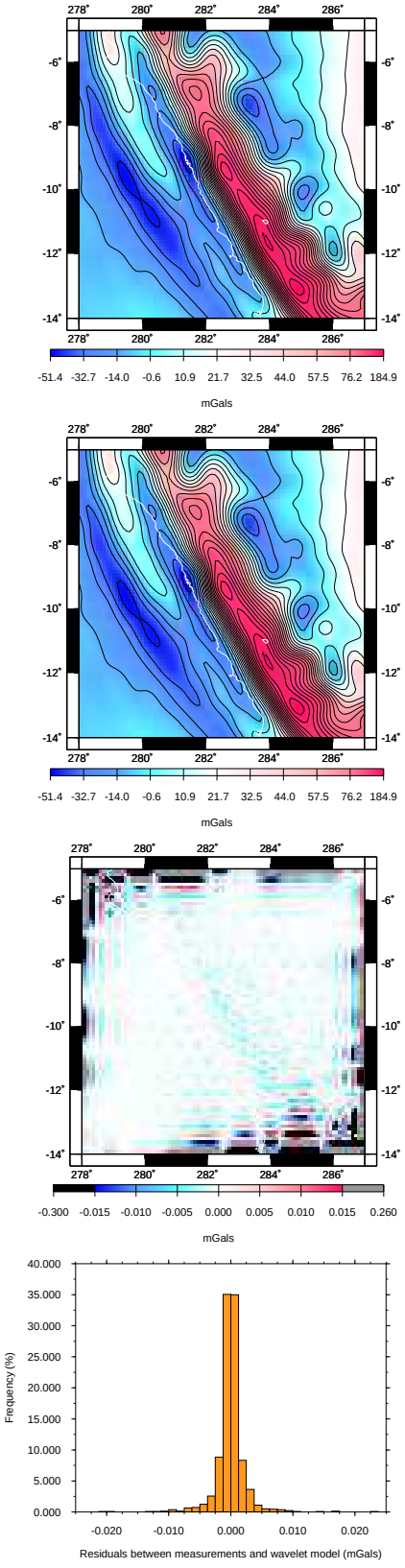

Figure 4: *From top to bottom* : EGM 96 gravity disturbances model; wavelet gravity disturbances model computed from the regular distribution of data; residuals between above wavelet model and EGM 96; residuals between wavelet model and synthetic data.

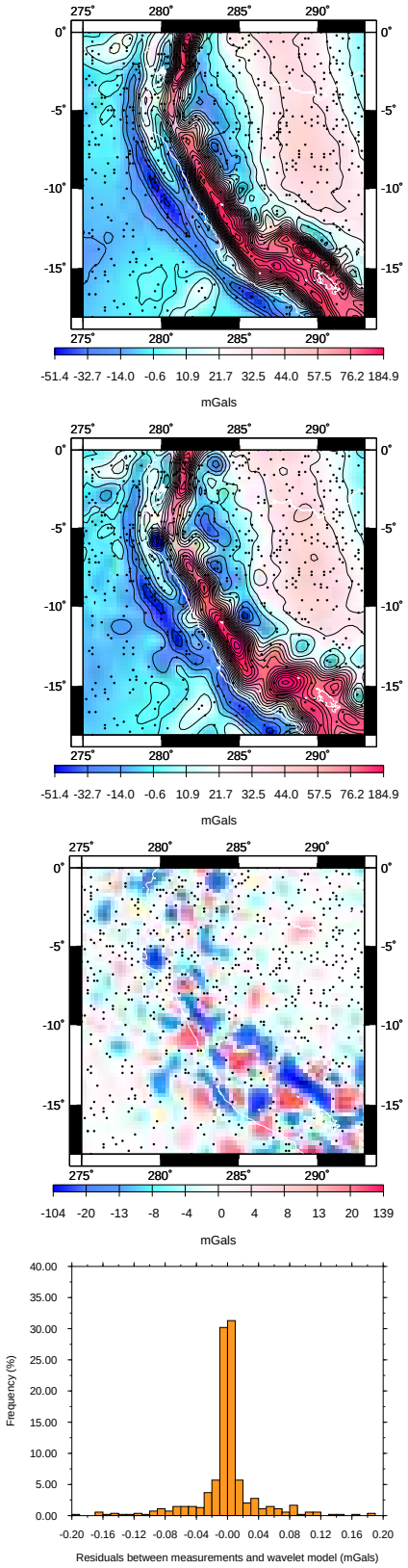

Figure 5: *From top to bottom* : EGM 96 gravity disturbances model (black dots represent the data); wavelet gravity disturbances model computed from the irregular distribution of data; residuals between above wavelet model and EGM 96; residuals between wavelet model and synthetic data.

datasets: the first one based on a satellite-derived gravity model, and the other one made of ground measurements, bringing the high frequency content.

References

Albertella, A., Sanso, F. and Sneeuw, N., 1999. Band-limited functions on a bounded spherical domain: the Slepian problem on the sphere. *J. of Geod.*, **73**, 436-447.

Chambodut, A., Panet, I., Mandea, M., Diament, M., Jamet, O., Holschneider, M.. Wavelet frames: an alternative to the spherical harmonics representation of potential fields. *Geophys. Journ. Int.*, submitted.

De Santis, A. and J.M., Torta, 1997. Spherical cap harmonic analysis : a comment on its proper use for local gravity field representation, *J. of Geod.*, **71**, 526-532.

Freeden, W., T., Gervens and M., Schreiner, M., 1998. Constructive Approximation on the Sphere (With Applications to Geomathematics), *Oxford Science Publication*, Clarendon Press, Oxford.

Holschneider, M., A., Chambodut and M., Mandea, 2003. From global to regional analysis of the magnetic field on the sphere using wavelet frames, *Phys. Earth Planet. Inter.*, **135**, 107-124.

Hwang, Ch., 1993. Spectral analysis using orthonormal functions with a case study on the sea surface topography. *Geoph. Journ. Int.*, **115**, 1148-1160.

Kaula, W.M., 1966. Theory of satellite geodesy, Waltham, Blaisdell.

Kenner, H., 1976. Geodesic math and how to use it, Berleley CA: University of California Press.

Lemoine, F.G. et al. 1998. The development of the joint NASA GSFC and the National Imagery and Mapping Agency (NIMA) geopotential model EGM96. NASA/TP - 1998 - 206861, Greenbelt, Maryland.

Mallat, S., 1999. A wavelet tour of signal processing. Academic Press, 2nd edition.

Martelet, G., Sailhac, P., Moreau, F., Diament, M., 2001. Characterization of geological boundaries using 1D wavelet transform on gravity data: Theory and application to the Himalayas. *Geophysics*, **66**, 4, 1116-1129.

Moritz, H., 1989. Advanced physical geodesy, Karlsruhe:Wichmann, 2. ed.

Sailhac, P., Galdeano, A., Gibert, D., Moreau, F., Delor, C.., 2000. Identification of sources of potential fields with the continuous wavelet transform: Complex wavelets and application to aeromagnetic profiles in French Guiana. *J. Geophys. Res.*, **105**, B8, 19455-19475.